JACS
JOURNAL OF THE AMERICAN CHEMICAL SOCIETY
Article
pubs.acs.org/JACS

Toward Multiple Conductance Pathways with Heterocycle-Based Oligo(phenyleneethynylene) Derivatives

Delia Miguel,[*,†] Luis Álvarez de Cienfuegos,[†] Ana Martín-Lasanta,[‡] Sara P. Morcillo,[†] Linda A. Zotti,[§] Edmund Leary,[‡] Marius Bürkle,[∥] Yoshihiro Asai,[∥] Rocío Jurado,[†] Diego J. Cárdenas,[⊥] Gabino Rubio-Bollinger,[#,⊗] Nicolás Agraït,[‡,#,⊗] Juan M. Cuerva,[*,†] and M. Teresa González[*,‡]

[†]Departamento de Química Orgánica, Universidad de Granada, C. U. Fuentenueva, Avda. Severo Ochoa s/n, E-18071 Granada, Spain

[‡]Fundación IMDEA Nanociencia, Ciudad Universitaria de Cantoblanco, E-28049 Madrid, Spain

[§]Departamento of Física Teórica de la Materia Condensada, Universidad Autónoma de Madrid, Ciudad Universitaria de Cantoblanco, E-28049 Madrid, Spain

[∥]Nanomaterials Research Institute, National Institute of Advanced Industrial Science and Technology (AIST), Tsukuba, Ibaraki 305-8568, Japan

[⊥]Departamento de Química Orgánica, Universidad Autónoma de Madrid, Ciudad Universitaria de Cantoblanco, E-28049 Madrid, Spain

[#]Departamento de Física de la Materia Condensada and Condensed Matter Physics Center (IFIMAC), Universidad Autónoma de Madrid, E-28049 Madrid, Spain

[⊗]Instituto "Nicolás Cabrera", Universidad Autónoma de Madrid, Ciudad Universitaria de Cantoblanco, E-28049 Madrid, Spain

Supporting Information

ABSTRACT: In this paper, we have systematically studied how the replacement of a benzene ring by a heterocyclic compound in oligo(phenyleneethynylene) (OPE) derivatives affects the conductance of a molecular wire using the scanning tunneling microscope-based break junction technique. We describe for the first time how OPE derivatives with a central pyrimidine ring can efficiently link to the gold electrode by two pathways presenting two different conductance *G* values. We have demonstrated that this effect is associated with the presence of two efficient conductive pathways of different length: the conventional end-to-end configuration, and another with one of the electrodes linked directly to the central ring. This represents one of the few examples in which two defined conductive states can be set up in a single molecule without the aid of an external stimulus. Moreover, we have observed that the conductance through the full length of the heterocycle-based OPEs is basically unaffected by the presence of the heterocycle. All these results and the simplicity of the proposed molecules push forward the development of compounds with multiple conductance pathways, which would be a breakthrough in the field of molecular electronics.

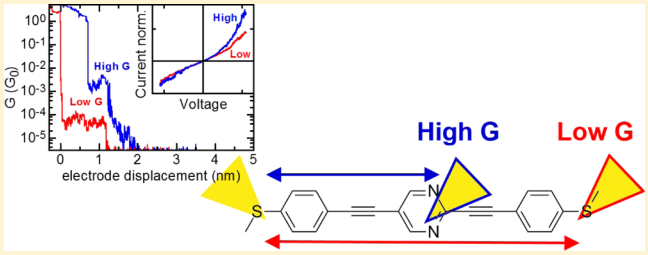

INTRODUCTION

The rich variety of phenomena observed in molecular electronics is largely based on specifically designed organic materials.[1] Going beyond bulk properties, new devices can be built, which allows for exploring and making use of the relationship between the molecular structure and the electrical transport properties of the materials at a single molecule level.[2] At present, molecular electronics takes advantage of the potent toolkit of organic chemists to build almost any conceivable structure, allowing the emergence of a large variety of π-conjugated organic molecules.[3] In this context, the discovery and understanding of new poly stable molecules with optimal geometry and states of significantly different conductance is an attractive goal. Very recently, some groups have demonstrated the possibility of using organic molecules with multiple pathways to connect electrode leads, mainly based on oligosilanes,[4] silicon cyclobutanes,[5] thiophene,[6] fullerene[7] derivatives and folded molecular wires.[8] Despite the success of specific structures, it would be valuable to extend these results to widely used *para*-phenylene ethylene-type oligomers (*p*-OPEs). These rigid structures have been extensively used as building blocks for 1D and 2D conjugated organic nanostructures.[9] As a proof of concept, we have prepared a family of OPE derivatives with three aromatic rings, and have studied the possibility of introducing a second conductive pathway directly via their central ring. To increase the binding properties of this ring, we tested the substitution of the prototypical benzene with

Received: June 1, 2015
Published: October 9, 2015

DOI: 10.1021/jacs.5b05637
J. Am. Chem. Soc. 2015, 137, 13818−13826

simple aromatic sulfur and nitrogen heterocycles (Scheme 1). Such heterocycles contain extra basic electron pairs compared

Scheme 1. Proposed Low (Whole Molecule) and High Conductance ("In-Backbone" Linkage) Channels in Heterocyclic OPE Derivatives

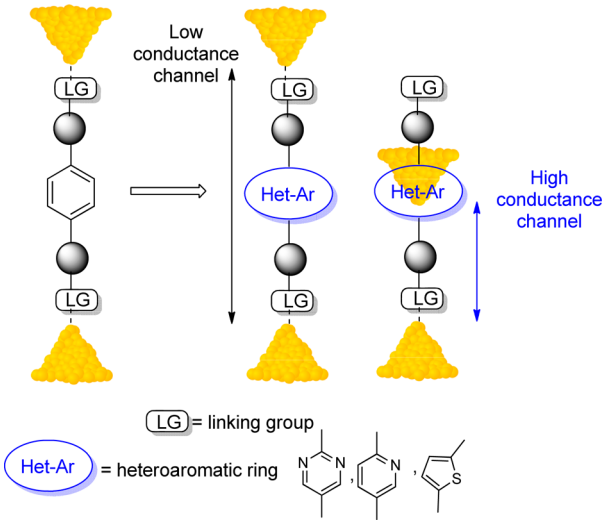

with benzene, which can be considered as new extra anchoring groups to metallic electrodes[10] placed halfway along the molecular backbone.

Additionally, heterocycles display other key differences with benzene: (a) they are less aromatic[11] and (b) the electron density within the ring can be higher or lower than in benzene. Remarkably, the effect of such differences on the electrical transport properties of OPE-containing heterocycles is practically unknown. Thus, for example, conductance studies of pyridines in the backbone[12] are mainly related with its use as viologen precursors for redox switches.[13] In this case, access to the influence on conductance values of neutral pyridines is not possible.[14,15] Moreover, the basic pairs are used to build the viologen moiety, and cannot be used as extra anchoring groups. Oligothiophenes[16] and alkynyloligothiophenes have also been extensively measured but the use of thiophene itself as linker[17] or a thiol derivative[18] precludes comparison with other systems using other more common linking groups.

In this paper, we study the family of compounds **1**–**7** including heterocycles (**2**–**4**, **6**–**7**) shown in Figure 1, using the break-junction technique. The thiophene aromatic group has shown interesting binding capabilities and for this reason compound **2** was selected for this study.[6] Likewise, pyridines have been extensively used as a linking group, and therefore, pyridine-containing model compound **3** was prepared.[19] Electrical transport studies of molecules containing polynitrogenated aromatic rings, such as **4**, are scarce, although some examples using pyrimidines have been described.[20] Shorter compounds **5**, **6**, and **7** were prepared as controls.

Our results allowed us to arrive at two main conclusions. On the one hand, we found that the existence of extra basic pairs present in some heterocycles (**4**) successfully promotes the in-backbone linking to the electrodes. This fact paves the way to future compounds with multiple stable pathways, practically inexistent in the field of molecular electronics, in a general and simple way. On the other hand, we observed that the replacement of CH groups in the OPE central ring with

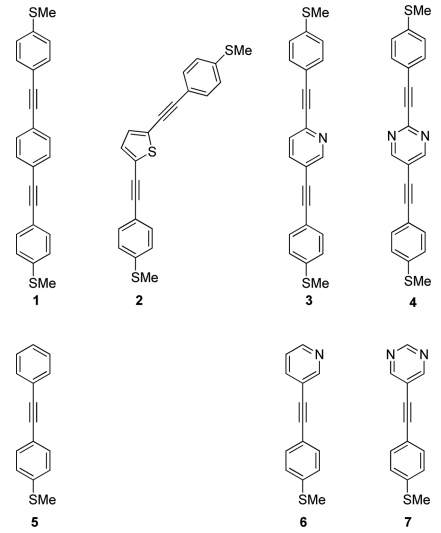

Figure 1. Chemical structure of *p*-OPE derivatives molecular wires.

nitrogen or sulfur atoms has little influence on the end-to-end conductance of the OPE. This observation is also supported by theoretical calculations. Henceforth, the existing proposed devices based on OPEs can be easily modified to incorporate new functionalities owing to the presence of basic electron pairs.

RESULTS AND DISCUSSION

We initially prepared methylsulfide-functionalized *p*-OPEs **1**–**7** using the Sonogashira cross-coupling reaction[21] between the commercially available mono- or dihalogenated aromatic compounds and 4-ethynylphenyl methyl sulfide[22] (Scheme S1 in the Supporting Information).

The electrical transport properties of these substances were explored with the break-junction (BJ) technique using a scanning tunneling microscope (STM).[19a] Details are described in the Experimental Section below. During the experiment, we record thousands of traces of the conductance variation produced when a gold tip is moved vertically out of contact with a gold substrate (G vs z traces). These traces often display plateaus at $G_0 = 2e^2/h$, which signal that a contact of just one gold atom is formed between the tip and the substrate. When continuing the electrode separation, new plateaus appear if a molecular junction forms with one or a few molecules bridging the opened gap between tip and the substrate. The conductance at which the plateau appears is the conductance of the molecular junction. To determine the typical junction conductance for each compound, we build one- and two-dimensional conductance histograms with more than 5000 traces. When many of the individual G vs z traces display plateaus around the same conductance value, a clear peak (prominence) will be formed in the corresponding 1D (2D) histogram. The typical junction conductance is obtained as the mean value of this peak.

Unsubsituted OPE Dimethylsulfide 1. First, we characterize the behavior of the reference compound **1**. Its corresponding 1D and 2D conductance histograms are shown in Figures 2a and 3a. It is well-known that the choice of binding group can have a strong influence on the outcome of the break-junction method.[23] To assess the efficiency of the methyl sulfide group, we have compared the conductance against two other common binding groups: amines and thiols. The

DOI: 10.1021/jacs.5b05637
J. Am. Chem. Soc. 2015, 137, 13818–13826

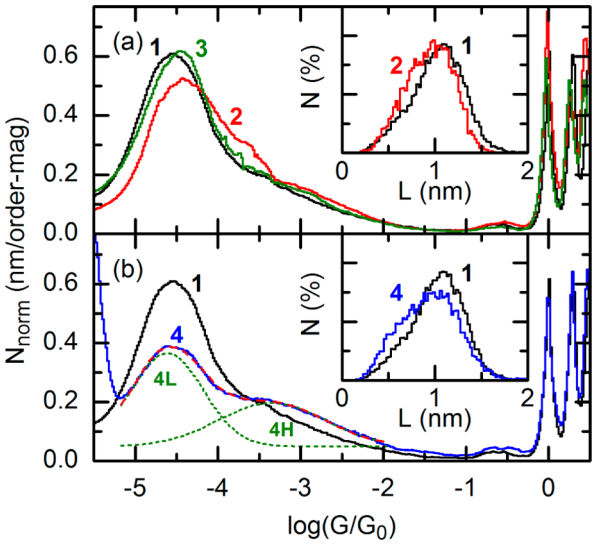

Figure 2. Comparison of the 1D conductance histograms of all traces with plateaus for compounds **1**–**4**. The dashed red line in panel (b) is the fit to the histogram of **4** of the sum of two gaussians (depicted individually by dotted green lines). The plateau-length distributions for **1**, **2**, and **4** are also compared in the insets.

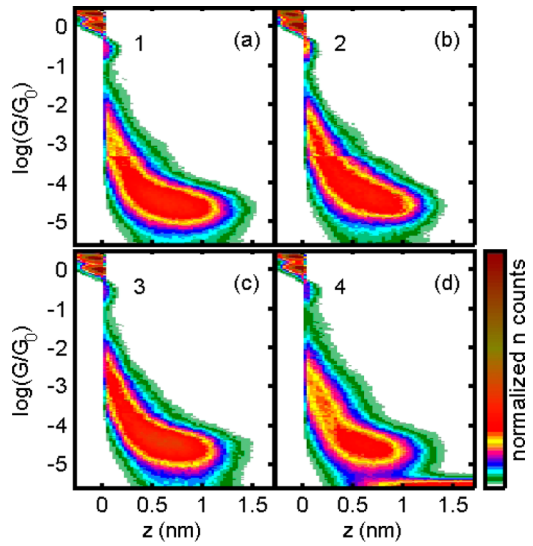

Figure 3. Corresponding 2D conductance histograms to those of Figure 2, built from all traces with plateaus for compounds **1**–**4**. Abrupt changes in the number of counts at $\log(G/G_0) = -3.6$ are due to the gain change during the measurement.

comparison of this derivative with the analogous OPE–diamine and dithiol is described in detail in the Supporting Information (Figures S1 and S2), showing that the conductance values for the thiomethyl terminated compound are only slightly lower than for the amine, and 1 order of magnitude lower than for OPE–dithiol. Plateau-length, L, distributions are quite similar for SMe and NH_2, while the distribution for SH is shifted approximately 0.3 nm to higher values. In our case, thus, we do not observe longer plateaus for the thiomethyl terminated compound than for the amine terminated one as previously reported.[24] Our results indicate, however, that despite the fact that SH and SMe groups bind through sulfur atoms, the binding properties differ significantly. These differences can be ascribed to the fact that thiols bind covalently to gold, losing the terminal hydrogen atom. In the case of the methylsulfide group, the terminal methyl group cannot be removed by attachment to gold, so the interaction of the sulfur atom must be through one of the lone pairs. This makes the behavior of the group more like the amine, which also binds via a lone pair interaction.

Comparison with Heterocycle-Based OPEs 2–4. Next, we compared the conductance of compound **1** with the OPE derivatives containing heteroatoms. The formation of new molecular junctions with molecules bonded to one of the electrodes through the S or N atoms at the middle ring should produce new shorter plateaus at different conductance values from those of compound **1**. Figures 2 and 3 show that while the derivatives with one heteroatom in their structure (**2** and **3**) produce results equivalent to those of compound **1**, compound **4**, with two nitrogen atoms in its structure, does produce a new peak of higher conductance and shorter plateau length.

Focusing first on compounds **2** and **3**, we see that the histogram of compound **3** is almost identical to that of **1**, both having a conductance peak centered at $\log(G/G_0) = -4.5 \pm 0.5$, where the uncertainty is given by the half width at half-maximum of the peak. We find a slightly larger, but still small, conductance difference for compound **2**, with a peak centered at $\log(G/G_0) = -4.3 \pm 0.5$, which is concurrent with a slight shift of the plateau length distribution to lower values (Figure 2a inset). These results are compatible with what we would expect from the shorter end-to-end length for this compound. The mean values for the conductance and plateau length of all the studied compounds are summarized in Table S1 and Figure S4, Supporting Information.

For compound **4**, with two nitrogen atoms in its structure, two peaks are observed. One of them is in the same region as for compounds **1**–**3** ($\log(G/G_0) = -4.6 \pm 0.5$), and, remarkably, a new broad peak is observed between $\log(G/G_0) = -4$ and -2.5, centered at a conductance approximately 1 order of magnitude higher than the first ($\log(G/G_0) = -3.4 \pm 0.75$) (see individual traces with plateaus in both ranges in Figure S6, Supporting Information). The plateau-length distribution is different too, giving a higher percentage of shorter plateaus (Figure 2b inset). The 2D histogram of Figure 3d shows that these new shorter plateaus are those in the high conductance region. Both conductance and plateau-length histograms can be reproduced as the sum of two gaussians with quite good overlap (Figure 2b and Figure S5). In the 2D histograms of Figure 3, compounds **2** and **3** do also have faint features between $\log(G/G_0) = -4$ and -2.5, which reflects the minor presence of conductance plateaus in that region. However, due to the fact that this feature is also present in compound **1**, we conclude that a single heteroatom does not change behavior of the parent compound. We will come back to this point later in the text. We note here that, in order to rule out the possibility of the high conductance plateaus being due to the presence of short impurities, we synthesized **4** following a second synthetic route (see Supporting Information). In this new route, any potential subproduct with linking groups would be much longer than the length of compound **4**.

As we proposed in the introduction, we hypothesize that the new plateaus observed for compound **4** could correspond to junctions in which the nitrogen-containing aromatic ring is in direct contact with one of the electrodes, and the electrons flow directly from it to one of the thiomethyl ether groups. In this scenario, the corresponding broader conductance distribution (labeled by 4H in Figure 2b) could be explained by the

DOI: 10.1021/jacs.5b05637
J. Am. Chem. Soc. 2015, 137, 13818–13826

influence of the position of second half of the molecule (not bridging the electrodes) in the direct coupling between the pyrimidine group of compound **4** and the gold electrode, which will likely produce larger junction-to-junction variations than if the pyrimidine were at an end of the compound.

This hypothesis would mean that the presence of the nitrogen atoms in those specific positions adds new functionality to the molecule allowing a second "in backbone" linking group. This result would be analogous to that recently described by T. A. Su et al.[5] using cyclobutylsilanes as "in backbone" linkers. The nitrogen-containing heterocycles presented here are more easily introduced into the structure using conventional Sonogashira protocols, and the nature of their bonding to gold is well established. This strategy of introducing heteroaromatic rings as in-backbone linkers is quite interesting as it can also be applied in longer molecules to produce multiple conductance pathways. In addition, the basic electronic pairs responsible for this phenomenon could be temporally masked (i.e., by coordination to metals), allowing new functionality in the molecule.

The generally low conductance values observed for these compounds suggest a strong mismatch between the Fermi level of gold and both the HOMO and LUMO levels of the OPE. The close appearance of the histograms observed for compounds **1**, **2** and **3** suggest that this mismatch is not significantly alleviated by the heteroatom inclusion. Neither the expected increase of the energy of the HOMO level for compound **2** nor the decrease of the energy of the LUMO level for compound **3** have significant consequences on the conductance at low experimental bias voltage *V*. To shed light on how introducing S and N heterocycles affects the electrical conduction across an OPE, we have performed theoretical calculations based on a combination of density functional theory (DFT) and Green's function techniques. Further information about the method employed is given below in the Theoretical Details section.

We have first analyzed compounds **1**−**4** in the gas phase. In particular, we found that replacement of the central phenyl ring of compound **1** with a nitrogen-containing heterocycle as in compound **3** or **4** slightly lowers the energy of the HOMO and LUMO orbitals but does not change their spatial extension significantly (the wave functions and the corresponding energy values are shown in Figure S9 of the Supporting Information). The presence of the nitrogen atom introduces additional states localized on the central ring which, however, lie at a lower energy (corresponding to the HOMO − 2). A similar scenario applies to molecule **2**, for which the HOMO − 3 is localized on the central sulfur heterocycle, while the HOMO is delocalized over the whole molecule and lies at a slightly higher energy than the HOMO of compound **1**.

Subsequently, we have built metal−molecule−metal junctions incorporating each of the compounds **1**−**4**. After exploring various binding configurations, we have found that the S atom of the SMe group prefers to bind to undercoordinated Au atoms, in agreement with what was previously reported by Kamenetska et al.[25] In Figure 4d, we show the low-bias transmission curves for compounds **1**−**4** in a top binding configuration (Figure 4a).

The electronic transport is found to take place through the HOMO of each molecule, the energetic alignment of which follows the same trend as in the gas phase. The contribution of the orbitals localized on the central heterocycles (HOMO − 2 for compound **3** and **4** and HOMO − 3 for compound **2**) is

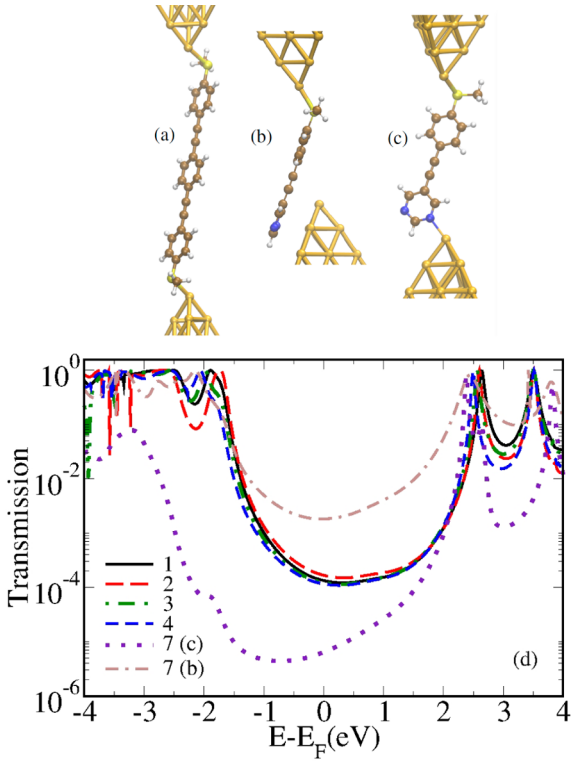

Figure 4. (a−c) Studied geometries: compound **1** in the top binding configuration (a) and compound **7** in two different geometries, where the pyrmidine unit is physisorbed on the face of a Au(111) pyramid (b) or attached to it through a N−Au bond (c). (d) Low-bias transmission for compounds **1**−**4** in the top-binding geometry (a) and for compound **7** in the two geometries shown in (b) and (c).

negligible, as the channel decomposition of the transmission shows (Figure S10 of the Supporting Information). The conductance values, evaluated as the transmission at the Fermi level, do not show significant differences, in agreement with the experimental measurements. It can be thus observed that the overall effect of replacing the central benzene ring of an OPE with an S or N heterocycle is similar to that of replacing the H atoms of the same ring with functional groups.[26,27]

Short Analogue Results 5−7. To check our hypothesis about the two conductive paths of compound **4**, we synthesized the model compounds **5**, **6**, and **7**, which could be considered as the short analogues of structurally similar **1**, **3** and **4** (Figure 1). For compound **5**, which is terminated at one end with just a phenyl group, we observed that the *G* vs *z* traces do not display flat plateaus as for the other compounds, but just a continuous conductance decay. This decay is slower than the tunneling background (see Figure S6, Supporting Information) and gives rise to the long and broad protuberance in the 2D conductance histogram shown in Figure 5b. This fact suggests that the benzene ring is not enough to form a stable bond to gold. The observed slow *G* decay is probably the result of weakly π-stacked junctions that take place by only one phenyl group.[19d]

In contrast, the peaks in the histograms of compounds **6** and **7** revealed that both were able to form stable molecular linkages, which indicates that the coupling of the aromatic ring to gold is enhanced by the presence of nitrogen. In fact, the rate of success in forming molecular junctions for these compounds remained at around 70−80% as in the case of the long analogs (see Table S1, Supporting Information). The conductance peak for compound **7** is centered at $\log(G/G_0) = -3.8 \pm 0.38$, which

DOI: 10.1021/jacs.5b05637
J. Am. Chem. Soc. 2015, 137, 13818−13826

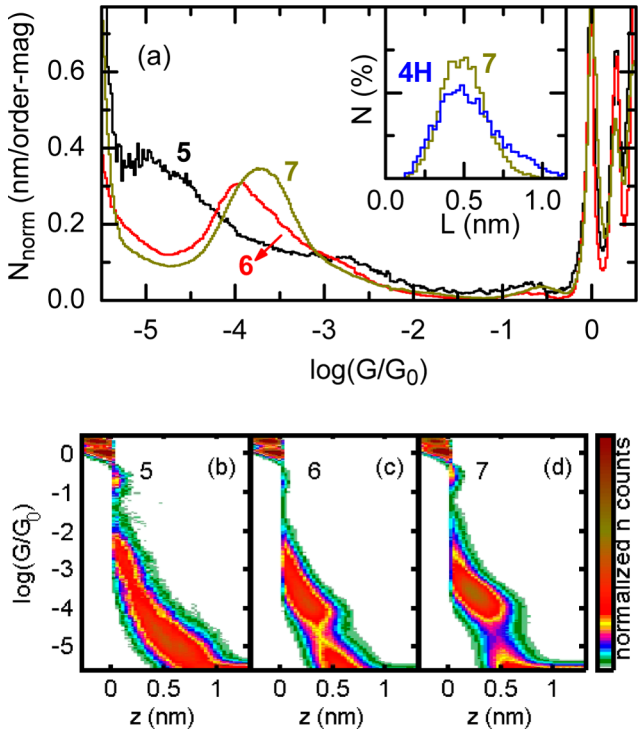

Figure 5. 1D (a) and 2D (b–d) conductance histograms of all traces with plateaus for compounds **5**, **6**, and **7**. The plateau length distribution of compound **7** is compared in the inset with that of the high conductance plateaus of compound **4** (**4**H).

is close but slightly lower than the higher conductance peak in **4**. This fact suggests that, in the in-backbone linkage for compound **4**, the half of the molecule which is not bridging the gap does play a role, and the linkage is therefore not identical to that of **7**. Probably, this part lies flat on the gold electrode, contributing to the stability of the junction. In fact, although it is not expected to provide the main contribution to the electrical current, its proximity to the gold could still affect the energetic alignment of the molecular orbitals and, consequently, the conductance.

To characterize further the behavior of compound **4**, and ease its comparison with compound **7**, we classified the recorded G vs z traces for compound **4** into groups according to the conductance value at their plateaus. Using $\log(G/G_0) = -3.8$ as the threshold conductance, we defined sets of traces with plateaus at high conductance (**4**H), low conductance (**4**L), or with plateaus in both ranges (**4**H&L) (details are described in the Data Analysis section below, and results are shown in Figure S7, Supporting Information). We found that a clean separation of traces was not possible due to the large conductance overlap between the two peaks shown in Figure 2b. Nevertheless, the process allowed us to establish that at least 30% of the junctions formed for compound **4** produce plateaus of shorter length and higher conductance than those clearly observed for **1**. It also allows us to compare the length of the high conductance plateaus of **4**(**4**H) with those of compound **7**. This comparison is displayed in the inset of Figure 5a, and shows that both distributions mostly overlap. This result strongly supports our hypothesis that these molecules can bind to the electrodes using two different linking groups: the expected thiomethyl group (low conductance) and the pyrimidine central ring (high conductance).

From the theoretical point of view, we have studied junctions incorporating compound **7** in two kinds of binding geometry: one in which the pyrimidine ring is physisorbed on the face of the Au(111) pyramide and the molecule interacts with the gold surface via its π-system (Figure 4b) and one in which the same ring is connected to the electrode via a N–Au bond (Figure 4c). The corresponding transmission curves are also shown in Figure 4d. In both cases, the current flows through the HOMO, which is delocalized over the whole molecule, albeit with a higher weight on the benzene ring. However, in the geometry of Figure 4b, this orbital is much more hybridized than in the other case, as the parallel position of the nitrogenated ring with respect to the face of the pyramid allows a better coupling of the π system with the gold states. In the case of Figure 4c instead, the heterocycle is perpendicular to the face of the gold pyramid, leading to a smaller coupling of the same orbital and, consequently, to a lower conductance. The binding energy of the geometry of Figure 4b was found to be 0.44 eV stronger than the other one, in agreement with what was found for bypiridine molecules in similar geometries.[28] The fact that the physisorbed geometry gives rise to a higher conductance than the corresponding longer compounds **1**–**4** suggests that the signature observed in the experimental measurements corresponds to this kind of configuration, with the pyrimidine group parallel to the electrode surface, rather than to that shown in Figure 4c.

We note here that we ran our separation process also for compound **1** and found that short plateaus similar to those of compound **4** are also present for it in the high conductance range in around 9% of the traces with plateaus. This suggests the phenyl rings might be enough to form in-backbone bonds in some cases. However, the low percentage of traces in comparison with that of compound **4** shows that the phenyl ring is much less effective in binding than the pyrimidine group, to the point that the presence of these high conductance plateaus was not evident in the global histograms of Figure 2. Interestingly, the same is true for compound **3**, even when its short analogue, compound **6**, displays 78% of traces with plateaus between $\log(G/G_0) = -4.3$ and -3.3. This is probably due to steric hindrance, and indicates that one anchoring group is not enough to stabilize the crowded in-backbone junction with the central ring laying parallel to the electrode surface, as in the configuration of Figure 4b for compound **7**. Even in the scenario in which the heterocycle ring is parallel to the gold, there is the possibility to form a direct N–Au bond through the lone pair which can act to anchor the group to the electrode surface. This keeps the ring close to the surface. This stabilizing effect is obviously higher in compound **4** than in compound **3** for having two N atoms rather than only one and totally absent in the case of compound **1**. We see then that the pyrimidine subunit is essential for favoring the binding through an in-backbone moiety.

Current versus Voltage Curves. As a final test, we repeated our measurements for compound **4** and **7** recording current vs voltage curves (IV curves) along the conductance plateaus of both compounds (see details in the Experimental Section). Figure 6a shows examples of individual G vs z traces for compound **4**, for which we have measured IV curves up to $V = \pm 1.1$ V along the plateaus. The averaged IV curve for each plateau is displayed in the inset, while the final average from all the measured IV curves for compound **4** (**4**L and **4**H) and **7** are shown in Figure 6b. To facilitate the comparison between the IV-curve profiles, we have scaled the averaged curves by the

DOI: 10.1021/jacs.5b05637
J. Am. Chem. Soc. 2015, 137, 13818–13826

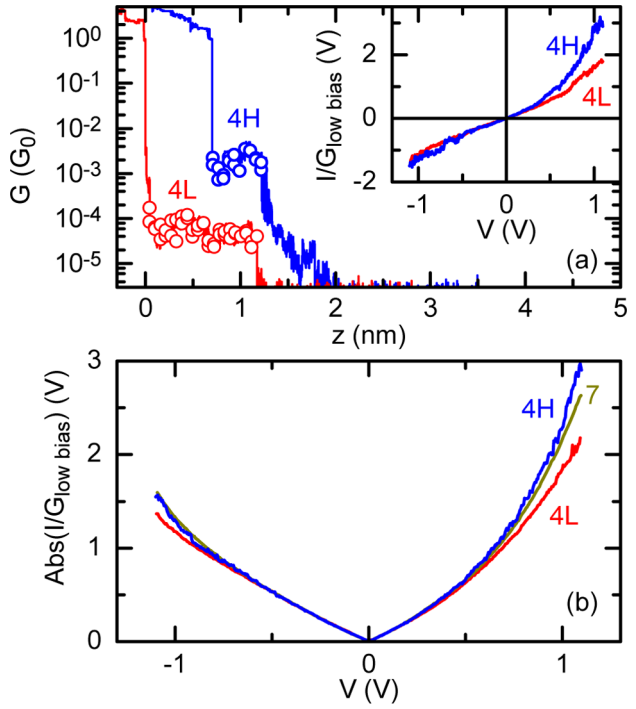

Figure 6. (a) Two G vs z traces for compound **4**. The empty circles indicate the positions at which IV curves have been collected. The inset shows the averaged IV curve for each plateau. (b) Overall averaged of all the IV curves recorded for the configurations of **4** and for **7**.

conductance close to zero bias voltage and, in Figure 6b, we show the absolute value of the current. Due to the different nature of the thiomethyl and pyrimidine binding groups, we expect more asymmetry in the coupling to the electrodes of compound **7**, or the in-backbone binding of compound **4** (**4**H), when compared with the end-to-end binding configuration of compound **4** (**4**L). This would translate into a larger asymmetry in the IV curves when reversing V. This is indeed observed in the IV curves of Figure 6, where a percentage of the IV curves has been flipped so that their high current branch lies always at positive voltages (see Experimental Section below). In the figure, the results for **4**H and **7** are very close, which again supports our hypothesis of an in-backbone binding as the origin of the **4**H plateaus. In addition, two features of the measured IV curves are worth emphasizing. The first is that even for the **4**L configuration we observed some asymmetry with a typical ratio between the absolute value of the current for voltages of different signs (rectification ratio) of 1.6, similarly as previously observed for biphenyldithiol.[29] The second is that, for compound **7**, which can only form junctions with two different binding groups at each extreme, the asymmetry is only slightly increased, with a rectification ratio that does not reach 2. In fact, for all three cases, we recorded a large percentage of rather symmetric IV curves, with a rectification ratio below 1.5 (see Figure S8 in Supporting Information). The observed low effect of a different coupling to the electrodes suggests again that the Fermi level of gold is close to the center of the HOMO–LUMO gap and far from the molecular orbitals as shown in Figure 4d. This is also supported by the overall limited curvature of the IV curves which remain rather linear up to almost 1 V, as it would be expected from the flat transmission region in the energy interval at the center of the HOMO–LUMO gap in the curves of Figure 4d.

CONCLUSIONS

In this paper, we propose a new strategy to develop compounds with controlled multiple conductance pathways by introducing in-backbone linkers in easy-to-tune OPE derivatives. To this end, a family of heterocycle-based OPE derivatives was synthesized and their conductance was measured by STM-BJ. We observed that linking groups previously used to create molecular junctions, such as pyridine and thiophene, are not good as in-backbone linkers. In those cases, we mainly observed one conductance peak corresponding to the whole molecule. Remarkably, pyrimidine **4** derivative showed two well-spaced conductive channels. The new high conductance channel derives from an efficient linking process of the pyrimidine ring to the gold electrodes, thus shortening the conductive pathway and increasing the conductance 1 order of magnitude. This fact could be confirmed using shorter analogues in which the conductance values and plateau-length distributions are very similar to the high conductance peak obtained in **4**. IV curves and theoretical calculations are also in agreement with these findings. Therefore, the combination of thiomethyl ethers as anchoring groups placed at both ends of the molecule and pyrimidine group at the center of the OPE has allowed the conduction through two distinct pathways: low conductance sulfur to sulfur pathway and high conductance nitrogen to sulfur pathway. The same strategy used here could now be easily applied to produce longer compounds with multiple conductance pathways.

We could also conclude that the global conductance of OPEs was unaffected by the substitution of benzene central ring neither by electron-rich nor electron-deficient heterocyclic rings. Taking advantage of this, it would be possible to modify existing benzene-based derivatives in the field of molecular electronics by introduction of heterocycles in their structures without changing the global electronic behavior of the system.

EXPERIMENTAL SECTION

Spectroscopic Data of Derivatives 1–7. General procedures for the Sonogashira couplings and copies of NMR spectra are described in the Supporting Information. Spectroscopic data of compounds **5**[30] and **6**[31] were identical as previously reported. Data of derivatives **1**–**4**, and **7** are below.

Compound 1: pale brown solid; ^{1}H NMR (500 MHz, CD_2Cl_2) δ 7.53 (s, 2H), 7.48 (d, J = 8.6 Hz, 2H), 7.25 (d, J = 8.5 Hz, 2H), 2.53 (s, 3H); ^{13}C NMR (125 MHz, CD_2Cl_2) δ 140.1 (C), 131.9 (CH), 131.4 (CH), 125.7 (CH), 123.0 (C), 119.0 (C), 91.0 (C), 89.0 (C), 15.2 (CH_3); HRMS (EI, 70 eV) m/z calcd for $C_{24}H_{18}S_2$ $[M]^+$, 370.0850; found, 370.0853.

Compound 2: pale yellow solid; ^{1}H NMR (500 MHz, CD_2Cl_2) δ 7.46 (d, J = 8.6 Hz, 2H), 7.25 (d, J = 8.6 Hz, 2H), 7.19 (s, 1H), 2.53 (s, 3H); ^{13}C NMR (125 MHz, CD_2Cl_2) δ 140.4 (C), 131.8 (CH), 131.6 (CH), 125.6 (CH), 125.5 (C), 118.5 (C), 93.9 (C), 82.1 (C), 15.0 (CH_3); HRMS (EI, 70 eV) m/z calcd for $C_{22}H_{16}S_3[M]^+$, 376.0414; found, 376.418.

Compound 3: pale brown solid; ^{1}H NMR (600 MHz, CD_2Cl_2) δ 8.69 (s, 1H), 7.76 (d, J = 7.6 Hz, 1H), 7.49 (d, J = 8.2 Hz, 3H), 7.48–7.46 (m, 1H), 7.45 (d, J = 8.1 Hz, 2H), 7.22 (d, J = 7.3 Hz, 4H), 2.49 (s, 6H); ^{13}C NMR (151 MHz, CD_2Cl_2) δ 152.4 (CH), 141.9 (C), 141.2 (C), 140.8 (C), 138.3 (CH), 132.3 (CH), 132.0 (CH), 126.5 (CH), 125.7 (CH), 125.6 (CH), 119.4 (C), 118.4 (C), 118.0 (C), 94.0 (C), 90.7 (C), 88.9 (C), 86.1 (C), 15.0 (CH_3), 14.97 (CH_3); HRMS (EI, 70 eV) m/z calcd for $C_{22}H_{16}NS_2$ $[M]^+$, 371.0802; found, 371.0800.

Compound 4: brown solid; ^{1}H NMR (600 MHz, CD_2Cl_2) δ 8.84 (s, 1H), 7.59 (d, J = 8.2 Hz, 1H), 7.51 (d, J = 8.2 Hz, 1H), 7.28 (dd, J = 8.2, 1H), 7.27 (dd, J = 8.2, 1H), 2.54 (s, 3H); ^{13}C NMR (151 MHz,

DOI: 10.1021/jacs.5b05637
J. Am. Chem. Soc. 2015, 137, 13818–13826

CD_2Cl_2) δ 158.8 (CH), 150.5 (C), 142.2 (C), 141.5 (C), 132.8 (CH), 132.0 (CH), 125.6 (CH), 125.5 (CH), 117.9 (C), 117.8 (C), 117.0 (C), 97.4 (C), 89.4 (C), 88.5 (C), 82.9 (C), 14.94 (CH_3), 14.87 (CH_3); HRMS (EI, 70 eV) m/z calcd. for $C_{22}H_{16}N_2S_2[M]^+$, 372.0755; found, 372.0757. Elemental analysis calc for $C_{22}H_{16}N_2S_2$: C, 70.93; H, 4.33; N, 7.52; H, 17.22; obtained C, 70.81; H, 4.42; N, 7.65; S, 16.11 (see Supporting Information).

Compound 7: brown solid. ^{1}H NMR (300 MHz, CD_2Cl_2) δ 9.13 (s, 1H), 8.85 (s, 2H), 7.44 (d, J = 8.4 Hz, 2H), 7.21 (d, J = 8.4 Hz, 2H), 2.49 (s, 3H).^{13}C NMR (75 MHz, CD_2Cl_2) δ 158.6 (CH), 156.7 (CH), 141.2 (C), 132.1 (CH), 125.8 (CH), 117.9 (C), 96.4 (C), 82.5 (C), 15.3 (CH_3). HRMS (ESI) m/z calcd for $C_{13}H_{11}N_2S$ $[M + H]^+$, 227.0637; found, 227.0634.

Break-Junction Experiments. We used a home-built scanning tunneling microscope (STM), which has been previously described.[33] As substrate, we used commercial gold samples on quartz (Arrandee), and as tip, we used a freshly cut gold wire. The experiments were performed in air, after immersing the substrate in 10^{-5} M solutions of compounds **1**−**7** in CH_2Cl_2 for 2 min and then drying them. The use of more concentrated solution resulted in nonreliable measurements with a 100% of traces showing plateaus and a tunneling background with reduced barrier energy.

Along all the measurements, a bias voltage V of 200 mV was kept constant between the tip and the substrate, and a protection 200 kΩ resistor was placed in-series with the substrate-tip circuit. A linear current-to-voltage converter with two amplification stages was used to measure the current I in the circuit. Our gains in this work were 10^7 and 2×10^9 V/A, after the first and second stages, respectively, for compounds **1**−**3**, and 5.6×10^5 and 11.5×10^7 V/A for compounds **4**−**7**. These gains were selected to explore the maximum range of conductance according to the value of the conductance peaks of each compound.

Data Analysis. For each compound, we recorded several thousands of individual G vs z traces in different experimental runs changing to a new tip, substrate and in different days, and built one and two-dimensional histograms after separating the traces with plateaus from those without plateaus. These were built with more than 5000 traces, and summarize the results of at least 3 experimental runs with a similar rate of success, ranging from 65 to 85%. As reported elsewhere,[32] we observe variations in the histogram profile of a given compound in experiments with very different rates of success. This probably reflects that, at higher rates of success, a larger number of molecules is trapped in averaged between the electrodes (see also Figure S3, Supporting Information).

Our criterion to consider that a trace has a plateau is that, at any conductance below 0.5 G_0, a displacement Δz larger than 0.1 nm is needed to produce a change in conductance of $\Delta\log(G/G_0) = 0.1$. As reference, the typical displacement needed for gold−gold tunneling in air is 0.02 nm. For compound **4**, we separated the traces in those with plateaus between $\log(G/G_0)$= −5.3 and −3.8 (**4**L), those with traces between $\log(G/G_0)$ = −3.8 and −1 (**4**H), and those with traces in both intervals (**4**L and H).

The plateau length of each trace, L, is calculated as the total displacement Δz needed to change the junction conductance from 0.5 to 5×10^{-6} G_0 for compounds **1**−**3**, and the traces with low conductance plateaus of compound **4**; and from 0.5 to 5×10^{-5} G_0 for compounds **5**−**7**, and the traces with high conductance plateaus of compound **4**.

Current versus Voltage Curves. For compounds **4** and **7**, G vs z traces were measured stopping the movement of the STM each 0.06 nm to record IV curves. The bias voltage was ramped between −1.1 and 1.1 V, and both the ramping-up and ramping-down curves were collected.

To determine the typical asymmetry of the IV curves, we forced the higher conductance branch of each IV curve to be at positive voltages, by flipping the whole IV curve when required. We flipped 51 ± 8% of the IV curves in all the cases. This means that for half of the original IV curves the higher conductance branch is toward a voltage sign, and for the other half toward the other, as we would expect, as there is not intrinsic difference between our electrodes. The IV curves were scaled by the conductance close to zero bias voltage ($G_{\text{low bias}}$) obtained from the slope of the IV curves in the (−0.2 V, 0.2 V) interval, where they are practically linear.

Theoretical Details. We carried out calculations based on density functional theory (DFT) to determine the geometry and electronic structure of the molecular junctions as well as their transport properties. The DFT calculations were performed by the quantum chemistry code TURBOMOLE,[33] using a split-valence basis set with polarization functions for all non hydrogen atoms[34] and the BP86 exchange-correlation functional.[35]

We first carried out geometry optimizations of all molecules in the gas phase and analyzed their electronic structure. The gold−molecule−gold junctions were then built by placing the relaxed structures between two Au_{20} clusters and by performing a new optimization of the molecule and the 4 innermost Au atoms on each side of the junction. Subsequently, further gold layers were added to the optimized structures in order to extend the size of both clusters to around 60 atoms and to describe correctly the metal−molecule charge transfer as well as the corresponding level alignment. Finally, single-point calculations were performed on these extended systems and the low-bias transmission of the junctions was computed in the spirit of the Landauer formalism using Green's function techniques.[36] The HOMO−LUMO gap was corrected by the DFT+Σ method.[37,38] The DFT-D2 correction for the dispersive forces[39] was included in the optimization of the geometries and the evaluation of the corresponding binding energies.

■ ASSOCIATED CONTENT

Supporting Information

The Supporting Information is available free of charge on the ACS Publications website at DOI: 10.1021/jacs.5b05637.

General procedures for Sonogashira couplings and alternative route for the synthesis of compound **4**; copies of ^{1}H NMR and ^{13}C NMR spectra of new compounds **1**−**4**, **7**; copies of elemental analysis, HPLC chromatogram and UV of pyrimidine derivative **4**; comparison of the conductance histogram for compound **1** with those for OPE−dithiol and diamine; plateau lengths for all the studied compounds; fits to the plateau length distribution for compounds **1** and **4**; examples of individual G vs z traces for compounds **4**, **5** and **7**; histograms for the separated G vs z traces with only high or low conductance plateaus; 2D histograms of the scaled IV curves for compound **4**; table with the percentage of traces with plateaus and plateau length for the study compounds; theoretical details about molecular orbitals in the gas phase, channel decomposition of the transmission and HOMO−LUMO gap corrections (PDF)

■ AUTHOR INFORMATION

Corresponding Authors

*dmalvarez@ugr.es
*jmcuerva@ugr.es
*teresa.gonzalez@imdea.org

Notes

The authors declare no competing financial interest.

■ ACKNOWLEDGMENTS

This research was funded by the Regional Government of Andalucía (projects P12-FQM-790 and FQM2012-2721), MINECO (project CTQ2011-22455, MAT2011-25046 and MAT2014-57915-R), the CAM (S2013/MIT-2850 and S213/MIT-3007), and the EC through the FP7 ITNs MOLESCO

DOI: 10.1021/jacs.5b05637
J. Am. Chem. Soc. 2015, 137, 13818−13826

(project 606728). S.P.M. and R.J. thank Regional Government of Andalucía, A.M.-L. thanks University of Granada and D.M. thanks Ministerio de Economía y Competitividad for their contracts. L.A.Z. was funded through the grant MAT2011-23627. M.B. was partly supported by a FY2012 (P12501) Postdoctoral Fellowship for Foreign Researchers from the Japan Society for Promotion of Science (JSPS) and by a JSPS KAKENHI, i.e., 'Grant-in-Aid for JSPS Fellows', Grant No. 24•02501. Y.A. is also thankful to another KAKENHI, i.e., Grant-in-Aid for Scientific Research on Innovation Areas "Molecular Architectonics: Orchestration of Single Molecules for Novel Functions" (#25110009). We thank fruitful discussions with Juan Carlos Cuevas.

REFERENCES

(1) Zimbovskaya, N. A.; Pederson, M. R. *Phys. Rep.* **2011**, *509*, 1−87.

(2) For recent general reviews see: (a) Bergfield, J. P.; Ratner, M. A. *Phys. Status Solidi B* **2013**, *250*, 2249−2266. (b) Fahrenbach, A. C.; Warren, S. C.; Incorvati, J. T.; Avestro, A.-J.; Barnes, J. C.; Stoddart, J. F.; Grzybowski, B. A. *Adv. Mater.* **2013**, *25*, 331−348. (c) Fuentes, N.; Martín-Lasanta, A.; Álvarez de Cienfuegos, L.; Ribagorda, M.; Parra, A.; Cuerva, J. M. *Nanoscale* **2011**, *3*, 4003−4014. (d) van der Molen, S. J.; Liljeroth, P. *J. Phys.: Condens. Matter* **2010**, *22*, 133001.

(3) Jenney, N. M.; Mayor, M.; Eaton, T. R. *Eur. J. Org. Chem.* **2011**, *2011*, 4965−4983.

(4) Su, T. A.; Li, H.; Steigerwald, M. L.; Venkataraman, L.; Nuckolls, C. *Nat. Chem.* **2015**, *7*, 215−220.

(5) Su, T. A.; Widawsky, J. R.; Li, H.; Klausen, R. S.; Leighton, J. L.; Steigerwald, M. L.; Venkataraman, L.; Nuckols, C. *J. Am. Chem. Soc.* **2013**, *135*, 18331−18334.

(6) Kiguchi, M.; Ohto, T.; Fujii, S.; Sugiyasu, K.; Nakajima, S.; Takeuchi, M.; Nakamura, H. *J. Am. Chem. Soc.* **2014**, *136*, 7327−7332.

(7) Moreno-García, P.; La Rosa, A.; Kolivoska, V.; Bermejo, D.; Hong, W.; Yoshida, K.; Baghernejad, M.; Filippone, S.; Broekmann, P.; Wandlowski, T.; Martín, N. *J. Am. Chem. Soc.* **2015**, *137*, 2318−2327.

(8) Chen, L.; Wang, Y.-H.; He, B.; Nie, H.; Hu, R.; Huang, F.; Qin, A.; Zhou, X.-S.; Zhao, Z.; Tang, B. Z. *Angew. Chem., Int. Ed.* **2015**, *54*, 4231−4235.

(9) For recent papers see: (a) Fan, Q.; Zhu, J.; Kuttner, J.; Hilt, G.; Gottfried, J. M. *Angew. Chem.* **2013**, *125*, 4766−4770. (b) Tang, Q.; Zhou, Z.; Chen, Z. *Nanoscale* **2013**, *5*, 4541−4583. (c) Oteyza, D. G.; Gorman, P.; Chen, Y.-C.; Wickenburg, S.; Riss, A.; Mowbray, D. J.; Etkin, G.; Pedramrazi, Z.; Tsai, H.-Z.; Rubio, A.; Crommie, M. F.; Fischer, F. R. *Science* **2013**, *340*, 1434−1437. (d) Kissel, P.; Erni, R.; Schweizer, W. B.; Rossell, M. D.; King, B. T.; Bauer, T.; Götzinger, S.; Schlüter, A. D.; Sakamoto, J. *Nat. Chem.* **2012**, *22*, 803−812.

(10) Although this goal can be achieved using functionalized benzenes, such functionalization is not always possible. Moreover, the basicity of the electron pairs can also differ by orders of magnitude. Thus, for example, the described pK_a value in water for thiophene is −10.2, thus considerably less basic than aliphatic amines (pK_a values around 9−10). In-between them, we can find nitrogenated aromatic heterocycles, such as pyridine and pyrimidine with pK_a values of 5.29 and 1.3, respectively.

(11) (a) Alonso, M.; Herradon, B. *J. Comput. Chem.* **2009**, *31*, 917−928. (b) Balaban, A. T.; Oniciu, D. C.; Katritzky, A. R. *Chem. Rev.* **2004**, *104*, 2777−2812.

(12) For other examples with pyridines as side chains see: (a) Ashwell, G. J.; Urasinska, B.; Wang, C.; Bryce, M. R.; Grace, I.; Lambert, C. J. *Chem. Commun.* **2006**, 4706−4708. (b) Ashwell, G. J.; Tyrrell, W. D.; Urasinska, B.; Wang, C.; Bryce, M. R. *Chem. Commun.* **2006**, 1640−1642. (c) Wang, C.; Batsanov, A.; Bryce, M. R.; Ashwell, G. J.; Urasinska, B.; Grace, I.; Lambert, C. J. *Nanotechnology* **2007**, *18*, 044005.

(13) (a) Li, Z.; Pobelov, H.; Han, B.; Wandlowski, T.; Blaszczyk, A.; Mayor, M. *Nanotechnology* **2007**, *18*, 044018. (b) Haiss, W.; van Zalinge, H.; Higgins, S. J.; Bethell, D.; Höbenreich, H.; Schiffrin, D. J.; Nichols, J. R. *J. Am. Chem. Soc.* **2003**, *125*, 15294. (c) Pobelov, I. V.; Li, Z.; Wandlowski, T. *J. Am. Chem. Soc.* **2008**, *130*, 16045−16054. (d) Leary, E.; Higgins, S. J.; van Zalinge, H.; Haiss, W.; Nichols, J. R.; Nygaard, S.; Jeppesen, J. O.; Ulstrup, J. *J. Am. Chem. Soc.* **2008**, *130*, 12204−12205. (d) Gittins, D. I.; Bethell, D.; Schiffrin, D. J.; Nichols, R. J. *Nature* **2000**, *408*, 67−69.

(14) Pyridine moiety has been also used as metal ligand to connect two molecular wires. Again, the pyridine effect on the conductance is masked by many other factors: (a) Park, J.; Pasupathy, A. N.; Goldsmith, J. L.; Chang, C.; Yaish, Y.; Petta, J. R.; Rinkoski, M.; Sethna, J. P.; Abruñas, H. D.; McEuen, P. L.; Ralph, D. C. *Nature* **2002**, *417*, 722−725. (b) Ng, Z.; Loh, K. P.; Li, L.; Ho, P.; Bai, P.; Yip, H. K. *ACS Nano* **2009**, *3*, 2103−2114. (c) Osorio, E. A.; Moth-Poulsen, K.; van der Zant, H. S. J.; Paaske, J.; Hedegard, P.; Flensberg, K.; Bendix, J.; Bjornholm, T. *Nano Lett.* **2010**, *10*, 105−110. (d) Zhou, X.-S.; Liu, L.; Fortgang, P.; Lefevre, A.-S.; Serra-Muns, A.; Raouafi, N.; Amatore, C.; Mao, B.-W.; Maisonhaute, E.; Schöllhorn, B. *J. Am. Chem. Soc.* **2011**, *133*, 7509−7516.

(15) Functionalized 2,2-bypyridines have been studied as potential NDR components, but in this case, the effect of the constituents controls the electrical transport through the global system: (a) Khondaker, S. I.; Yao, Z.; Cheng, L.; Henderson, J. C.; Yao, Y.; Tour, J. M. *Appl. Phys. Lett.* **2004**, *85*, 645−647. (b) Blum, A. S.; Kushmerick, J. G.; Long, D. P.; Patterson, C. H.; Yang, J. C.; Henderson, J. C.; Yao, Y.; Tour, J. M.; Shashidhar, R.; Ratna, B. R. *Nat. Mater.* **2005**, *4*, 167−172. (c) Keane, Z. K.; Ciszek, J. W.; Tour, J. M.; Natelson, D. *Nano Lett.* **2006**, *6*, 1518−1521. (d) Lörtscher, E.; Ciszek, J. W.; Tour, J.; Riel, H. *Small* **2006**, *2*, 973−977.

(16) (a) Leary, E.; Höbenreich, H.; Higgins, S. J.; van Zalinge, H.; Haiss, W.; Nichols, R. J.; Finch, C. M.; Grace, I.; Lambert, C. J.; McGrath, R.; Smerdon. *Phys. Rev. Lett.* **2009**, *102*, 086801. (b) Dell, E. J.; Capozzi, B.; Xia, J.; Venkataraman, L.; Campos, L. M. *Nat. Chem.* **2015**, *7*, 209−214. (c) Yamada, R.; Kumazawa, H.; Noutoshi, T.; Tanaka, S.; Tada, H. *Nano Lett.* **2008**, *8*, 1237−1240.

(17) Arroyo, C. R.; Tartuc, S.; Frisenda, R.; Seldenthuis, J. S.; Woerde, C. H. M.; Eelkema, R.; Grozema, F. C.; van der Zant, H. S. J. *Angew. Chem., Int. Ed.* **2013**, *52*, 3152−3155.

(18) (a) Dulic, D.; Pump, F.; Campidelli, S.; Lavie, P.; Cuniberti, G.; Filoramo, A. *Angew. Chem., Int. Ed.* **2009**, *48*, 8273−8276. (b) Yokota, K.; Taniguchi, M.; Tsutsui, M.; Kawai, T. *J. Am. Chem. Soc.* **2010**, *132*, 17364−17365.

(19) Pyridine moiety has been extensively used as linking group although the electrical transport characteristics are masked in all the cases by its interaction with the corresponding electrodes: (a) Xu, B.; Tao, N. J. *Science* **2003**, *301*, 1221−1223. (b) Xu, B.; Xiao, X.; Tao, N. J. *J. Am. Chem. Soc.* **2003**, *125*, 16164−16165. (c) Li, X.; Hihath, J.; Chen, F.; Masuda, T.; Zang, L.; Tao, N. J. *J. Am. Chem. Soc.* **2007**, *129*, 11535−11542. (d) Wu, S.; Gonzalez, M. T.; Huber, R.; Grunder, S.; Mayor, M.; Schönenberger, C.; Calame, M. *Nat. Nanotechnol.* **2008**, *3*, 569−574. (e) Wang, C.; Batsanov, A. S.; Bryce, M. R.; Martín, S.; Nichols, R. J.; Higgins, S. J.; García-Suarez, V. M.; Lambert, C. J. *J. Am. Chem. Soc.* **2009**, *131*, 15647−15654. (f) Kamenetska, M.; Quek, S. Y.; Whalley, A. C.; Steigerwald, M. L.; Choi, H. J.; Louie, S. G.; Nuckolls, C.; Hybertsen, M. S.; Neaton, J. B.; Venkataraman, L. *J. Am. Chem. Soc.* **2010**, *132*, 6817−6821. (g) Ie, Y.; Hirose, T.; Nakamura, H.; Kiguchi, M.; Takagi, N.; Kawai, M.; Aso, Y. *J. Am. Chem. Soc.* **2011**, *133*, 3014−3022. (h) Hong, W.; Manrique, D. Z.; Moreno-Garcia, P.; Gulcur, M.; Mishchenko, A.; Lambert, C. J.; Bryce, M.; Wandlowski, T. *J. Am. Chem. Soc.* **2012**, *134*, 2292−2304. (i) Ballman, S.; Härtle, R.; Coto, P.; Mayor, M.; Elbing, M.; Bryce, M.; Thoss, M.; Weber, H. B. arXiv: 1203.4128v12012. (j) Roldan, D.; Kaliginedi, V.; Cobo, S.; Kolivoska, V.; Bucher, C.; Hong, W.; Royal, G.; Wandlowski, T. *J. Am. Chem. Soc.* **2013**, *135*, 5974−5977. (k) Konishi, T.; Kiguchi, M.; Tasake, M.; Nagasawa, F.; Nabika, H.; Ikeda, K.; Uosaki, K.; Ueno, K.; Misawa, H.; Murakoshi, K. *J. Am. Chem. Soc.* **2013**, *135*, 1009−1014. (l) Manrique, D. Z.; Huang, C.; Baghernejad, M.; Zhao, X.; Al-Owaedi, O. A.; Sadeghi, H.; Kaliginedi, V.; Hong, W.; Gulcur, M.; Wandlowski, T.; Bryce, M. R.; Lambert, C. L. *Nat. Commun.* **2015**, *6*, 6389.

DOI: 10.1021/jacs.5b05637
J. Am. Chem. Soc. 2015, 137, 13818−13826

(20) (a) Diez-Pérez, I.; Hihath, J.; Lee, Y.; Yu, L.; Adamska, L.; Kozhushner, M. A.; Oleynik, I. I.; Tao, N. *Nat. Chem.* **2009**, *1*, 635−641. (b) Nakamura, H.; Asai, Y.; Hihath, J.; Bruot, C.; Tao, N. *J. Phys. Chem. C* **2011**, *115*, 19931−19938.
(21) (a) Chinchilla, R.; Najera, C. *Chem. Soc. Rev.* **2011**, *40*, 5084−5121. (b) Chinchilla, R.; Najera, C. *Chem. Rev.* **2007**, *107*, 874−922. (c) Sonogashira, K.; Tohda, Y.; Hagihara, N. *Tetrahedron Lett.* **1975**, *16*, 4467−4470.
(22) Sun, Y.; He, J.; Xu, Z.; Huang, G.; Zhou, X.; Zeller, M.; Hunter, A. D. *Chem. Commun.* **2007**, 4779−4781.
(23) Leary, E.; La Rosa, A.; González, M. T.; Rubio-Bollinger, G.; Agraït, N.; Martín, N. *Chem. Soc. Rev.* **2015**, *44*, 920−942.
(24) Frei, M.; Aradhya, S. V.; Hybertsen, M. S.; Venkataraman, L. *J. Am. Chem. Soc.* **2012**, *134*, 4003−4006.
(25) Kamenetska, M.; Koentopp, M.; Whalley, A. C.; Park, Y. S.; Steigerwald, M. L.; Nuckolls, C.; Hybertsen, M. S.; Venkataraman, L. *Phys. Rev. Lett.* **2009**, *102*, 126803.
(26) Bilan, S.; Zotti, L. A.; Pauly, F.; Cuevas, J. C. *Phys. Rev. B: Condens. Matter Mater. Phys.* **2012**, *85*, 205403.
(27) González, M. T.; Zhao, X.; Manrique, D. Z.; Miguel, D.; Leary, E.; Gulcur, M.; Batsanov, A. S.; Rubio-Bollinger, G.; Lambert, C. J.; Bryce, M. R.; Agräit, N. *J. Phys. Chem. C* **2014**, *118*, 21655−21662.
(28) Aradhya, S. V.; Frei, M.; Hybertsen, M. S.; Venkataraman, L. *Nat. Mater.* **2012**, *11*, 872−876.
(29) Guo, S.; Hihath, J.; Díez-Pérez, I.; Tao, N. *J. Am. Chem. Soc.* **2011**, *133*, 19189−19197.
(30) Huang, H.; Hong, L.; Jiang, H.; Chen, K. *J. Org. Chem.* **2008**, *73*, 6037−6040.
(31) Chowdhury, M. A.; Dong, Y.; Chen, Q.-H.; Abdellatif, K. R. A.; Knaus, E. E. *Bioorg. Med. Chem.* **2008**, *16*, 1948−1956.
(32) Arroyo, C. R.; Leary, E.; Castellanos-Gómez, A.; Rubio-Bollinger, G.; González, M. T.; Agraït, N. *J. Am. Chem. Soc.* **2011**, *133*, 14313−14319.
(33) Ahlrichs, R.; Bar, M.; Haser, M.; Horn, H.; Kolmel, C. *Chem. Phys. Lett.* **1989**, *162*, 165.
(34) Schafer, A.; Horn, H.; Ahlrichs, L. *J. Chem. Phys.* **1992**, *97*, 2571.
(35) Perdew, P. *Phys. Rev. B: Condens. Matter Mater. Phys.* **1986**, *33*, 8822.
(36) Pauly, F.; Viljas, J. K.; Huniar, U.; Hafner, M.; Wohlthat, S.; Burkle, M.; Cuevas, J. C.; Schon, G. *New J. Phys.* **2008**, *10*, 125019.
(37) Quek, S. Y.; Venkataraman, L.; Choi, H. J.; Louie, S. G.; Hybertsen, M. S.; Neaton, J. B. *Nano Lett.* **2007**, *7*, 3477−3482.
(38) For details see: Zotti, L. A.; Bürkle, M.; Pauly, F.; Lee, W.; Kim, K.; Jeong, W.; Asai, Y.; Reddy, P.; Cuevas, J. C. *New J. Phys.* **2014**, *16*, 015004.
(39) Grimme, S. *J. Comput. Chem.* **2006**, *27*, 1787−1799.

DOI: 10.1021/jacs.5b05637
J. Am. Chem. Soc. 2015, 137, 13818−13826